J|A|C|S
ARTICLES

Published on Web 08/10/2009

Nanoscale Zirconia as a Nonmetallic Catalyst for Graphitization of Carbon and Growth of Single- and Multiwall Carbon Nanotubes

Stephen A. Steiner III,*,[†] Theodore F. Baumann,[‡] Bernhard C. Bayer,[§]
Raoul Blume,[⊥] Marcus A. Worsley,[‡] Warren J. MoberlyChan,[‡] Elisabeth L. Shaw,[¶]
Robert Schlögl,[⊥] A. John Hart,[†,□] Stephan Hofmann,[§] and Brian L. Wardle[†]

Department of Aeronautics and Astronautics, Massachusetts Institute of Technology, Cambridge, Massachusetts 02139, Lawrence Livermore National Laboratory, Livermore, California 94551, Department of Engineering, University of Cambridge, Cambridge, UK CB3 0FA, Fritz-Haber-Institut der Max-Planck-Gesellschaft, D-14195 Berlin-Dahlem, Germany, Center for Materials Science and Engineering, Massachusetts Institute of Technology, Cambridge, Massachusetts 02139, and Department of Mechanical Engineering, University of Michigan, Ann Arbor, Michigan 48109

Received April 11, 2009; E-mail: ssteiner@alum.mit.edu

Abstract: We report that nanoparticulate zirconia (ZrO_2) catalyzes both growth of single-wall and multiwall carbon nanotubes (CNTs) by thermal chemical vapor deposition (CVD) and graphitization of solid amorphous carbon. We observe that silica-, silicon nitride-, and alumina-supported zirconia on silicon nucleates single- and multiwall carbon nanotubes upon exposure to hydrocarbons at moderate temperatures (750 °C). High-pressure, time-resolved X-ray photoelectron spectroscopy (XPS) of these substrates during carbon nanotube nucleation and growth shows that the zirconia catalyst neither reduces to a metal nor forms a carbide. Point-localized energy-dispersive X-ray spectroscopy (EDAX) using scanning transmission electron microscopy (STEM) confirms catalyst nanoparticles attached to CNTs are zirconia. We also observe that carbon aerogels prepared through pyrolysis of a Zr(IV)-containing resorcinol−formaldehyde polymer aerogel precursor at 800 °C contain fullerenic cage structures absent in undoped carbon aerogels. Zirconia nanoparticles embedded in these carbon aerogels are further observed to act as nucleation sites for multiwall carbon nanotube growth upon exposure to hydrocarbons at CVD growth temperatures. Our study unambiguously demonstrates that a nonmetallic catalyst can catalyze CNT growth by thermal CVD while remaining in an oxidized state and provides new insight into the interactions between nanoparticulate metal oxides and carbon at elevated temperatures.

Catalyst-assisted transformation of hydrocarbons into graphitic nanostructures is an important tool in the production of emerging electronics and structural materials. Carbon nanotubes (CNTs) in particular are of great interest for these areas and are now commonly produced through well-established thermal chemical vapor deposition (CVD) and other techniques.[1−3] The mechanism of CVD growth of CNTs, however, is still not fully understood. At a minimum, CVD growth of both single-wall and multiwall CNTs requires the use of a nanoparticle catalyst[4,5] which we now know is not limited in composition to the commonly employed transition metals Fe, Co, and Ni, but in fact can be composed of many metals.[4,6−16] This includes

---

[†] Department of Aeronautics and Astronautics, Massachusetts Institute of Technology.

[‡] Lawrence Livermore National Laboratory.

[§] University of Cambridge.

[⊥] Fritz-Haber-Institut der Max-Planck-Gesellschaft.

[¶] Center for Materials Science and Engineering, Massachusetts Institute of Technology.

[□] University of Michigan.

(1) Kong, J.; Cassell, A. M.; Dai, H. *Chem. Phys. Lett.* **1998**, *292*, 567–574.
(2) Hafner, J. H.; Bronikowski, M. J.; Azamian, B. R.; Nikolaev, P.; Rinzler, A. G.; Colbert, D. T.; Smith, K. A.; Smalley, R. E. *Chem. Phys. Lett.* **1998**, *296*, 195–202.
(3) Murakami, Y.; Miyauchi, Y.; Chiashi, S.; Maruyama, S. *Chem. Phys. Lett.* **2003**, *377*, 49–54.
(4) Dupuis, A.-C. *Prog. Mater. Sci.* **2005**, *50*, 929.
(5) Hofmann, S.; Sharma, R.; Ducati, C.; Du, G.; Mattevi, C.; Cepek, C.; Cantoro, M.; Pisana, S.; Parvez, A.; Cervantes-Sodi, F.; Ferrari, A. C.; Dunin-Borkowski, R.; Lizzit, S.; Petaccia, L.; Goldoni, A.; Robertson, J. *Nano Lett.* **2007**, *7*, 602–608.
(6) Wong, Y. M.; Wei, S.; Kang, W. P.; Davidson, J. L.; Hofmeister, W.; Huang, J. H.; Cui, Y. *Diamond Relat. Mater.* **2004**, *13*, 2105–2112.
(7) Wang, X.; Yue, W.; He, M.; Liu, M.; Zhang, J.; Liu, Z. *Chem. Mater.* **2004**, *16*, 799–805.
(8) Lee, C. J.; Lyu, S. C.; Kim, H.-W.; Park, J. W.; Jung, H. M.; Park, J. *Chem. Phys. Lett.* **2002**, *361*, 469–472.
(9) Yuan, D.; Ding, L.; Chu, H.; Feng, Y.; McNicholas, T. P.; Liu, J. *Nano Lett.* **2008**, *8*, 2576–2579.
(10) Bhaviripudi, S.; Mile, E.; Steiner, S. A., III.; Zare, A. T.; Dresselhaus, M. S.; Belcher, A. M.; Kong, J. *J. Am. Chem. Soc.* **2007**, *129*, 1516–1517.
(11) Yamada, M.; Kawana, M.-A.; Miyake, M. *Appl. Catal., A* **2006**, *302*, 201–207.
(12) Lee, S.-Y.; Yamada, M.; Miyake, M. *Carbon* **2005**, *43*, 2654–2663.
(13) Takagi, D.; Homma, Y.; Hibino, H.; Suzuki, S.; Kobayashi, Y. *Nano Lett.* **2006**, *6*, 2642–2645.

10.1021/ja902913r CCC: $40.75

Au,[10−12] Cu,[9,13,17] and Re,[15,16] which notably have poor bulk solubility for carbon and do not form stable carbides,[18,19] as well as the main group metal Sn[9] and the semiconductors Si, Ge, and SiC.[14] An even larger selection of transition metals (such as Ta), alloys (such as Al−Ti), and nonmetal substances (including $CuSiF_6$ and CeO_2) are known to act as graphitization catalysts for solid-state transformation of amorphous carbon.[20] Although catalytic graphitization is itself a complex process and occurs over a wider temperature range than typical CNT growth by CVD,[20] there is likely substantial mechanistic overlap between the two phenomena, for example in the types of intermediate bonding configurations and surface reactions involved.

In working to understand the necessary and sufficient attributes of effective nanotube catalysts, questions regarding the chemical state of the catalyst during CNT growth arise. The specific case of understanding the chemical state of iron during CNT growth raised the interesting debate of whether iron oxide (of some stoichiometry) or reduced iron (metallic or carbide) was the active catalyst species in that system. Recent direct observation of the chemical state of Fe during CNT growth through *in situ* X-ray photoelectron spectroscopy (XPS) by Mattevi et al. and Hofmann et al. revealed that it is a reduced species, not an oxide, that is the active catalyst.[21,22] Additionally, *in situ* X-ray diffraction (XRD) of catalyst particles during CNT growth from Fe nanoparticles by Nishimura et al. showed that upon introduction of carbon feedstock, the catalyst is deoxidized and that CNT growth is catalyzed by nanoparticles of iron carbides.[23] Sharma et al. further demonstrated the applicability of these observations at the single-nanoparticle level by atomic-level *in situ* TEM observations of CNT growth from Fe nanoparticles prepared by electron-beam-induced decomposition.[24] Although many metal oxides such as Fe_2O_3 and NiO are used to prepare substrates that do in fact catalyze CNT growth,[1,25] these oxides are almost certainly reduced prior to catalysis, either from being annealed in H_2 during ramp-up to the growth temperature or as observed by Nishimura et al., by localized carbothermic and/or H_2 reduction upon introduction of CNT feedstock gases.

Recently, Rümmeli et al. demonstrated that when placed under typical conditions for CVD growth of CNTs, nanoparticles of certain difficult-to-reduce metal oxides, some of which are often used as catalyst supports in CNT growth (such as alumina), create encapsulating graphene layers.[26] This finding raises questions regarding how commonly used catalyst supports affect CNT growth, or if in nanoparticle form materials used for supports could in fact themselves catalyze CNT growth. A recent study reports growth of SWNTs catalyzed by alumina nanoparticles, although it is not clear whether aluminum or an alumina coating on the nanoparticles is the active catalyst.[27] Two recent reports have also described growth of SWNTs from aluminum, but with limited characterization of the nanoparticles.[9,28] Together, these studies suggest that alumina itself may be a nanotube catalyst. Reports of growth of SWNTs from SiO_2 nanoparticles that result from scratches on SiO_2-coated Si wafers have also recently appeared, although again it remains speculative as to what the active catalyst species in these cases actually is.[29,30]

In this contribution, we report that nanoparticulate zirconia (ZrO_2) can both catalyze MWNT and SWNT growth by thermal CVD and catalyze transformation of solid amorphous carbon into graphitic nanoshells. Using *in situ* XPS analysis during CVD growth of CNTs from several substrates with zirconia, we show unambiguously, for the first time, that an oxide can catalyze CNT growth while remaining in an oxidized state during growth. We studied Si substrates coated with films of ZrO_2 deposited from liquid solutions and found that processing of these substrates by CVD resulted in substantial CNT growth. Depending on temperature and gas flow conditions used during CVD, these substrates demonstrated the ability to grow either SWNTs or MWNTs, including local vertically aligned “forest” morphologies which are indicative of high catalyst particle activity. We also investigated solid-state interactions between zirconia and carbon at elevated temperatures by preparing zirconia nanoparticle-doped carbon aerogels. Aerogels were produced through pyrolysis of Zr(IV)-containing resorcinol-formaldehyde polymer aerogels at 800 °C and exhibited the presence of fullerenic cage structures absent in undoped carbon aerogels. Subsequent CVD processing of zirconia-doped carbon aerogels also resulted in the growth of CNTs, apparently from zirconia particles embedded in the aerogel skeleton. *Ex situ* XRD and XPS analysis of Si and carbon aerogel substrates before and after CNT growth found no metallic zirconium or zirconium carbide present, suggesting that zirconia nanoparticles are not reduced by the hydrogen- and hydrocarbon-rich CVD atmospheres of CNT growth. *In situ* XPS analysis of low-pressure CVD growth of CNTs on Si and carbon aerogel substrates verified that no metallic zirconium or zirconium carbide arises at any point prior to, during, or following CVD growth of CNTs from zirconia nanoparticles.

In addition to demonstrating the interesting result that a metal oxide can exhibit these catalytic behaviors, zirconia offers unique promise as a useful catalyst for CNT growth. First, zirconia is nonmagnetic and, as we show, can catalyze SWNT growth, making it an interesting possible catalyst for electronics

---

(14) Takagi, D.; Hibino, H.; Suzuki, S.; Kobayashi, Y.; Homma, Y. *Nano Lett.* **2007**, *7*, 2272–2275.
(15) Steiner, S. A., III. Master’s Thesis, Massachusetts Institute of Technology, 2006.
(16) Ritschel, M.; Leonhardt, A.; Elefant, D.; Oswald, S.; Buchner, B. *J. Phys. Chem. C* **2007**, *111*, 8414–8417.
(17) Zhou, W.; Han, Z.; Wang, J.; Zhang, Y.; Jin, Z.; Sun, X.; Zhang, Y.; Yan, C.; Li, Y. *Nano Lett.* **2006**, *6*, 2987–2990.
(18) Okamoto, H.; Massalaski, T. B. *Bull. Alloy Phase Diagrams* **1984**, *5*, 378–379.
(19) Shunk, F. A., Ed. *Constitution of Binary Alloys*; McGraw-Hill: New York, 1969; p 155.
(20) Ôya, A.; Marsh, H. *J. Mater. Sci.* **1982**, *17*, 309–322.
(21) Mattevi, C.; Wirth, C. T.; Hofmann, S.; Blume, R.; Cantoro, M.; Ducati, C.; Cepek, C.; Knop-Gericke, A.; Milne, S.; Castellarin-Cudia, C.; Dolafi, S.; Goldoni, A.; Schloegl, R.; Robertson, J. *J. Phys. Chem. C* **2008**, *112*, 12207–12213.
(22) Hofmann, S.; Blume, R.; Wirth, C. T.; Cantoro, M.; Sharma, R.; Ducati, C.; Haevecker, M.; Zafeiratos, S.; Schnoerch, P.; Oestereich, A.; Teschner, D.; Albrecht, M.; Knop-Gericke, A.; Schloegl, R.; Robertson, J. *J. Phys. Chem. C* **2009**, *113*, 1648.
(23) Nishimura, K.; Okazaki, N.; Pan, L. J.; Nakayama, Y. *Jpn. J. Appl. Phys., Part 2* **2004**, *43*, L471–L474.
(24) Sharma, R.; Moore, E.; Rez, P.; Treacy, M. M. J. *Nano Lett.* **2009**, *9*, 689–694.
(25) Li, X.; Zuo, X.; Yuan, G.; Brown, A.; Westwood, A.; Brydson, R.; Rand, B. *J. Phys.: Conf. Ser.* **2005**, *26*, 308–311.
(26) Rümmeli, M. H.; Kramberger, C.; Grüneis, A.; Ayala, P.; Gemming, T.; Büchner, B.; Pichler, T. *Chem. Mater.* **2007**, *19*, 4105–4107.
(27) Liu, H.; Takagi, D.; Ohno, H.; Chiashi, S.; Chokan, T.; Homma, Y. *Appl. Phys. Express* **2008**, *1*, (014001-1)(014001-3).
(28) Esconjauregui, S.; Whelan, C. M.; Maex, K. *Carbon* **2008**, doi: 10.1016/j.carbon.2008.10.047.
(29) Liu, B.; Ren, W.; Gao, L.; Li, S.; Pei, S.; Liu, C.; Jiang, C.; Cheng, H.-M. *J. Am. Chem. Soc.* **2009**, *131*, 2082–2083.
(30) Huang, S.; Cai, Q.; Chen, J.; Qian, Y.; Zhang, L. *J. Am. Chem. Soc.* **2009**, *131*, 2094–2095.

applications. It is also relatively inexpensive compared to many other nonmagnetic CNT catalysts that have been reported (such as Au, Re, and Pt).[31] Second, zirconia offers the potential for facilitating CNT growth on historically challenging substrates, such as carbon, metals, and ceramics. Because of their reactivity at elevated temperatures, commonly used CNT catalysts (such as Fe, Co, and Ni) must often be stabilized with a metal oxide barrier to enable CNT growth on these substrates without causing damage to the substrate, thereby limiting many potential applications. Zirconia, however, is both a relatively inert oxide and apparently catalyzes CNT growth without dissolving carbon. Hierarchical nanoengineered filamentary composites are one potential application where such a catalyst would be valuable[32−35] and as a proof-of-concept we show here that zirconia can catalyze CNT growth on commercially available carbon fibers without causing pitting of the fibers. Third, ZrO_2 is not susceptible to oxidation, since it is already an oxide, and thus may be an advantageous catalyst for oxidative CNT growth conditions (i.e., water or alcohol growth). Furthermore, we and others[36] have observed that nanoparticulate ZrO_2 appears to be stable against carbothermic reduction at temperatures up to 1050 °C, suggesting it is also resistant against poisoning by carburization, which has been hypothesized to be a CNT growth termination mechanism for iron catalysts.

Methods

In the methods detailed below, great care was taken to prevent contamination by metals, especially iron. Clean, dedicated plastic and glass tools and containers were used for all stages of processing. Pyrolysis of aerogel samples and all CNT growth processes were conducted with an isolated set of new, dedicated quartz process tubes. Null CNT growth on ZrO_2-free Si substrates verified the absence of catalyst contamination in the CVD systems used. XPS analysis of the substrates used also verified that no Fe, Co, Ni, or other obvious potential catalysts were present before or after CVD processing.

Preparation of ZrO_2-Coated Si Substrates. All Si substrates used had a 200−300 nm layer of thermal SiO_2. Si substrates with Al_2O_3 supports were prepared through e-beam evaporation or RF sputter deposition of solid stoichiometric Al_2O_3. Si substrates with oxynitride support were prepared using a vertical thermal reactor followed by annealing. Saturated solutions $ZrOCl_2 \cdot 8H_2O$ in 2-propanol were prepared by adding 322 mg of $ZrOCl_2 \cdot 8H_2O$ to 20.0 g of 2-propanol, sonicating for ~5 min, and allowing nanoparticles to form over the course of 4−5 d. These solutions were then stirred and used for dip-coating or drop-casting zirconia nanoparticles onto Si wafers.

Preparation of ZrO_2-Doped Carbon Aerogels. ZrO_2-doped carbon aerogels and undoped control carbon aerogels were prepared using sol−gel processing through the ion-exchange technique developed for preparing metal-doped carbon aerogels, described elsewhere.[37−39] Briefly, the potassium salt of 2,4-dihydroxybenzoic acid was polymerized with formaldehyde in water to form a mesoporous K^+-doped resorcinol−formaldehyde polymer gel. Potassium carboxylate moieties throughout the gel structure act as ion-exchange sites, allowing the gel to be doped with other ions (such as transition metal ions) by exchanging the gel liquor with an aqueous ionic salt. Prior to ion exchange, the gel was purified by exchanging the gel liquor with deionized water. Ion exchange of K^+ for zirconyl was then performed by soaking the gel in a solution of saturated aqueous $ZrOCl_2 \cdot 8H_2O$ (Fluka, ≥99.0%, <0.4 μg/mg known CNT catalysts[40]). To serve as a control, an undoped gel was prepared by exchanging K^+ for H^+ through soaking in aqueous 0.1 *N* HCl. The gels were then purified and prepared for supercritical drying through multiple solvent exchanges (three exchanges per solvent, one exchange per 24 h) first with deionized water, then acetone, and finally liquid CO_2. The gels were then supercritically dried from CO_2 ($T_c = 31.1$ °C, $P_c = 72.9$ atm, $T_{max} = 50$ °C, $P_{max} = 100$ atm) to afford zirconyl-doped and undoped resorcinol−formaldehyde polymer aerogels, respectively. Finally, the aerogels were pyrolyzed under a flow of 200 sccm Ar at 800 or 1050 °C for 10.5 h, affording mesoporous carbon aerogels. In the case of the zirconyl-doped samples, the aerogels were found to be homogenously laced with polydisperse ZrO_2 nanoparticles encased in fullerenic nanoshells. The undoped aerogels exhibited a typical amorphous carbon structure only.

ZrO_2−Catalyzed Growth of CNTs. Thermal CVD growth of CNTs was performed on several different substrates, listed in Table 1.

Atmospheric thermal CVD was performed in a three-zone Lindberg/Blue M furnace with a 62-cm heated length using 50-mm inner diameter fused quartz process tubes with a length of 138 cm. Samples in this system were placed directly in the quartz tube between 50% and 75% of the heated length. Gases used were all ultrahigh purity grades (99.999%, Airgas, US). Low-pressure CVD growth for *in situ* XPS analysis was performed at the BESSY synchrotron in the end station of the FHI-MPG. (*Note that the term "low-pressure" refers to subatmospheric CVD, however these same conditions are considered "high-pressure" for XPS*). Samples in this system were transferred into a reaction cell and placed into differentially pumped stages of the lens system of a hemispherical analyzer (Phoibos 150, SPECS) ~2 mm away from the aperture. A focused IR laser was used for sample heating. Temperature readings were taken from a thermocouple spot-welded in the vicinity of the sample and, as such, an underestimation of up to ~100 °C may have occurred. The CVD atmosphere was constantly monitored by a mass spectrometer attached via a leak valve.

Atmospheric pressure CVD was performed with methane and ethylene feedstocks (Table 2). Low-pressure CVD employing acetylene was used for the *in situ* XPS analysis (Table 2). For atmospheric pressure growths, Si substrates were processed with both methane and ethylene conditions; carbon aerogel and carbon fiber samples were only processed using ethylene growth conditions at atmospheric pressure. *In situ* XPS analysis was performed for zirconia on Si with alumina support and zirconia-doped carbon aerogel.

Characterization. Si-based substrates were characterized by scanning electron microscopy (SEM), *ex situ* X-ray photoelectron spectroscopy (XPS), *in situ* XPS during CNT growth, transmission electron microscopy (TEM), point-localized energy-dispersive X-ray spectroscopy (EDAX) under scanning transmission electron microscopy (STEM), and Raman spectroscopy. ZrO_2-doped carbon aerogels were characterized by powder X-ray diffraction (XRD), *ex situ* XPS, *in situ* XPS during CNT growth, SEM, TEM, point-

---

(31) *Mineral Commodity Summaries*; U.S. Department. of the Interior, U.S. Geological Survey: Reston, VA, 2008; Vol. 19, pp 2−193.

(32) Qian, H.; Bismarck, A.; Greenhalgh, E. S.; Kalinka, G.; Shaffer, M. S. P. *Chem. Mater.* **2008**, *20*, 1862–1869.

(33) Garcia, E. J.; Wardle, B. L.; Hart, A. J.; Yamamoto, N. *Compos. Sci. Technol.* **2008**, *68*, 2034–2041.

(34) Downs, W. B.; Baker, R. T. K. *J. Mater. Res.* **1995**, *10*, 625–633.

(35) Yamamoto, N.; Hart, A. J.; Garcia, E. J.; Wicks, S.; Duong, H. M.; Slocum, A. H.; Wardle, B. L. *Carbon* **2009**, *47*, 551–556.

(36) Sacks, M. D.; Wang, C.-A.; Yang, Z.; Jain, A. *J. Mater. Sci.* **2004**, *39*, 6057–6066.

(37) Baumann, T. F.; Fox, G. A.; Satcher, J. H., Jr.; Yoshizawa, N.; Fu, R.; Dresselhaus, M. S. *Langmuir* **2002**, *18*, 7073–7076.

(38) Baumann, T. F.; Fu, R.; Cronin, S.; Dresselhaus, G.; Dresselhaus, M. S.; Satcher, J. H., Jr. *Langmuir* **2005**, *21*, 2647–2651.

(39) Steiner, S. A., III.; Baumann, T. F.; Satcher, J. H., Jr.; Kong, J.; Dresselhaus, M. S. *Langmuir* **2007**, *23*, 5161–5166.

(40) Trace cation analysis (available from Sigma-Aldrich): Ca ≤100 mg/kg; Cd ≤5 mg/kg; Co ≤5 mg/kg; Cr ≤10 mg/kg; Cu ≤5 mg/kg; Fe ≤10 mg/kg; K ≤50 mg/kg; Mg ≤5 mg/kg; Mn ≤5 mg/kg; Na ≤50 mg/kg; Ni ≤5 mg/kg; Pb ≤10 mg/kg; Ti ≤50 mg/kg; Zn ≤5 mg/kg.

Table 1. Summary of Control and Catalyst Substrates Evaluated for Catalytic Activity Towards CNT Growth

substrate type	control substrate	substrate(s) with catalyst
Si wafer, (100) orientation, 200−300 nm thermal SiO_2	unmodified Si wafer with 200−300 nm thermal SiO_2	wafer dip-coated or drop-cast with saturated solution of $ZrOCl_2 \cdot 8H_2O$ in 2-propanol
Si wafer, (100) orientation, 200−300 nm thermal SiO_2 and 10 nm alumina	unmodified Si wafer with 200−300 nm thermal SiO_2 and 10 nm alumina	wafer dip-coated or drop-cast with saturated solution of $ZrOCl_2 \cdot 8H_2O$ in 2-propanol
Si wafer, (100) orientation, 100 nm silicon oxyntride	unmodified Si wafer with 100 nm silicon oxynitride	wafer dip-coated or drop-cast with saturated solution of $ZrOCl_2 \cdot 8H_2O$ in 2-propanol
carbon aerogel	acid-neutralized (undoped) carbon aerogel	ZrO_2-doped carbon aerogel (6−8 nm mean ZrO_2 particle size)
unsized carbon fibers (Hexcel, AS4C 3k tow)	unmodified carbon fiber	carbon fibers dip-coated with saturated solution of $ZrOCl_2 \cdot 8H_2O$ in 2-propanol

Table 2. Summary of CVD Conditions Evaluated for CNT Growth from Zirconia Catalysts

feedstock	pressure	ramp	soak	growth	cool down
CH_4	atmospheric	ambient to 900 °C at 20 °C min^{-1}; 400 sccm He	0−10 min; 200 sccm H_2	15 min; 500 sccm CH_4, 100 sccm H_2	400 sccm He
C_2H_4	atmospheric	ambient to 750 °C at 50 °C min^{-1}; 400 sccm He	0−10 min; 400 sccm He, 1600 sccm H_2	10 min; 400 sccm C_2H_4, 400 sccm He, 1600 sccm H_2	400 sccm He
C_2H_2	low-pressure	ambient to ~530 °C at ~125 °C min^{-1}; 0.1 mbar H_2	15 min; 0.1 mbar H_2, followed by 20 min under 10^{-7} mbar vacuum	10 min; 10^{-2} mbar C_2H_2 only, followed by 20 min C_2H_2:H_2 mixture (1:5 ratio) at 0.2 mbar	under 10^{-7} mbar vacuum or 0.1 mbar H_2

localized EDAX under STEM, and Raman spectroscopy. Carbon fiber substrates were analyzed by SEM. XRD patterns were obtained using a PANalytical X'Pert Pro MPD with RTMS detector using Cu Kα radiation, a voltage of 45 kV, and a current of 40 mA. Phase identification and crystallite size determination were made using MDI Jade 7 equipped with the ICCD database. *Ex situ* XPS spectra were obtained on an AXIS Ultra DLD Spectrometer (Kratos Analytical Ltd., UK) using Al Kα radiation (energy = 1486.6 eV) in a chamber with a base pressure of 5×10^{-9} torr. For the carbon aerogels, XPS samples were prepared either by grinding the material into a fine powder and adhering to adhesive copper tape or by adhering monoliths directly to copper tape. The copper tape was mounted on a sample holder using double-sided adhesive carbon tape. Silicon substrates were directly mounted on the sample holder with carbon tape. All measurements were performed using an X-ray power of 150 W (15 kV and 10 mA), a pass energy of 10 eV, and an analysis area of 750 μm × 350 μm. A charge neutralizer was not used. Charge correction for carbon aerogel samples was not performed as no charging effect was observed; charge correction for silicon substrates was performed using peaks from SiO_2 or Al_2O_3 supports as reference points. High pressure *in situ* XPS spectra were collected in normal emission geometry at photon energies of 500 eV with a spectral resolution of ~0.3−0.4 eV. At these photon energies, the electron mean free path is ~10.5 Å. The analysis area was ~100 μm × 1 mm. Background correction was performed using a Shirley background. Spectra were fitted following the Levenberg−Marquardt algorithm to minimize the χ^2 value. Peak shapes were modeled using asymmetric Doniach−Sunjic functions convolved with Gaussian profiles. High-resolution scanning electron microscopy (HRSEM) was performed with a JEOL 6320 microscope and FEI Philips XL30 sFEG operating at 14 kV for carbon aerogel samples, 5 kV for carbon fiber samples and MWNT Si substrates, and 2.5 kV for samples from the *in situ* XPS analysis. High-resolution transmission electron microscopy (HRTEM) of carbon aerogels and derived nanotube composites was performed on a JEOL JEM-200CX operating at 200 kV. HRTEM and STEM of CNTs grown during *in situ* XPS experiments was performed on a JEOL 2010F operating at 200 kV equipped with an INCA system for performing EDAX. Raman spectra were obtained using a custom-built micro-Raman spectrometer operating at an excitation wavelength of 647 nm with a laser power of 25 mW and a collection time of 5 s. Peak fitting was performed using CasaXPS operating in Raman analysis mode. Peak shapes were modeled using an asymmetric Lorentzian line shape convolved with a Gaussian profile with tail exponents $\alpha = 1$ and $\beta = 1$ and Gaussian width $m = 2$ (program line shape LA(1,1,2)).

Results and Discussion

Growth of CNTs from zirconia on Si substrates was first evaluated by drop-casting a saturated solution of $ZrOCl_2 \cdot 8H_2O$ in 2-propanol onto Si wafers with a silicon oxynitride barrier. Following pretreatment under hydrogen and CVD processing of these wafers with ethylene feedstock at 750 °C, bundles of aligned CNTs ("mini-forests") could be observed at various locations on these wafers with SEM (Figure 1). While much of these wafers exhibited no growth, growth was in high yield where it was observed. Also observable on these wafers were cracked platelets, clusters, and films of zirconia, upon which the mini-forests and other long (>5 μm) CNT bundles were observed. Similar results were observed for zirconia on alumina and silica.

To understand whether zirconia or a reduced zirconium species (resulting from high-temperature exposure to hydrogen and hydrocarbons, for example) serves as the CNT growth

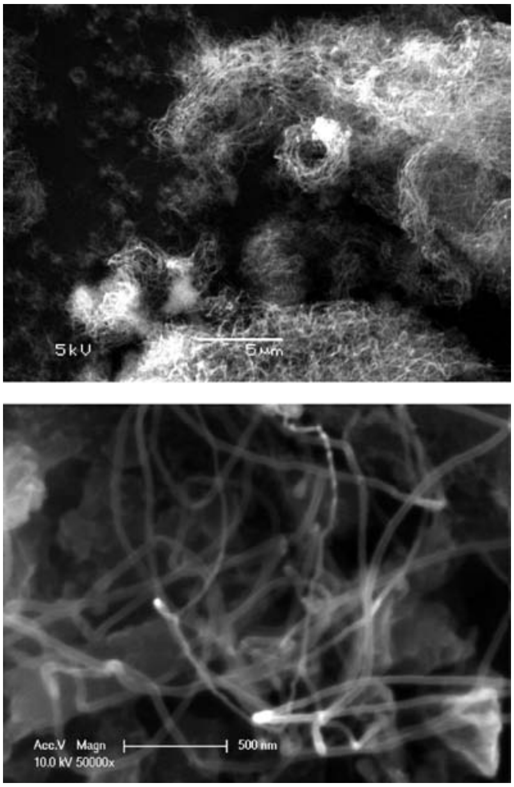

Figure 1. (*Top*) SEM of bundles of aligned CNTs catalyzed by ZrO_2 on silicon oxynitride support using ethylene feedstock at 750 °C. (*Bottom*) Close-up of large-diameter MWNTs extending from a cluster of zirconia particles.

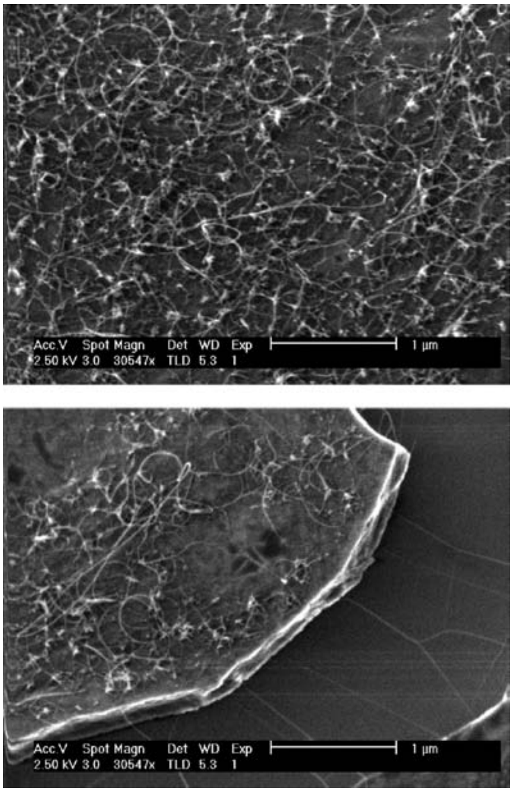

Figure 2. (*Top*) SEM images of CNTs grown from zirconia on a Si wafer with 10 nm alumina support, analyzed by XPS *in situ* during CVD. (*Bottom*) CNTs grown atop a platelet of zirconia on Si wafer during the *in situ* XPS analysis.

catalyst on these substrates, zirconia-coated wafers were analyzed by XPS *ex situ* of CVD growth. Both prior to and following exposure of the wafers to the CVD growth conditions, no metallic Zr or ZrC was found to be observable and instead only high-binding energy chemistries in the range expected for ZrO_2 were found. These observations are substantiated by the understanding of ZrO_2 chemistry at high temperatures in the literature. ZrO_2 is known to not be reduced by H_2, even at temperatures of 1500 °C and higher.[41] Additionally, carbothermic reduction of ZrO_2 does not yield Zr metal but instead results in the formation of ZrC,[42] and Sacks et al. have reported that carbothermic reduction of even nanocrystalline ZrO_2 to ZrC under Ar only begins at temperatures around 1200 °C[36]—much higher than the growth temperatures used in this study. Considering the phase diagrams of bulk $ZrO_2-Al_2O_3$ and ZrO_2-SiO_2, no significant reaction with the support is expected to occur at the conditions for CVD growth of CNTs. The phase diagram for the ZrO_2-SiO_2 system[43] shows that at <1000 °C, monoclinic ZrO_2 plus zircon ($ZrSiO_4$) is the favorable phase configuration. However, if zircon were forming during the CVD growth conditions, the XPS spectrum would show an additional silicon chemistry superimposed over the signal for SiO_2 in the Si 2p region, as well as a specific shift in the Zr 3d region to a higher binding energy by ~1 eV,[44,45] neither of which is found. Likely, in the inherently reductive environment of CNT growth, such a reaction between oxides would be inhibited. Similarly in the $ZrO_2-Al_2O_3$ system,[43] only a mixture of the separate oxides (i.e., no phase transition) is expected at both 750 and 900 °C (up to 1150 °C).

To verify the hypothesis that zirconia itself is serving as the CNT growth catalyst, we performed an *in situ* XPS analysis of low-pressure CVD growth of CNTs from ZrO_2. Figure 2 shows SEM images of CNTs grown from ZrO_2 on a Si substrate from this experiment. A substantial yield of CNTs was observed within the XPS analysis area by SEM, easily identifiable atop platelets of zirconia on the substrate surface. Figure 3 shows the progression of the C 1s and Zr 3d regions of the XPS spectra from this sample after heating in hydrogen, during growth with acetylene and H_2, and after CVD during cool-down in vacuum. Prior to introduction of hydrogen (not shown), a high-binding energy chemistry of Zr centered at 182.6 eV is initially observed, corresponding to the presence of electron-withdrawing oxychloride and alkoxide on the surface. Upon introduction of hydrogen, the Zr 3d signal shifts to a lower binding energy, corresponding to formation of zirconia.[46−49] Two pairs of spin−orbit-split peaks corresponding to two phases of zirconia can be resolved, one phase with the Zr $3d_{5/2}$ peak at 182.5 eV

---

(41) McTaggart, F. K. *Nature* **1961**, *191*, 1192.
(42) Berger, L.-M.; Gruner, W.; Langholf, E.; Stolle, S. *Int. J. Refract. Met. Hard Mater.* **1999**, *17*, 235–243.
(43) *Phase Diagrams for Zirconium and Zirconia Systems*; Ondik, H. M.; McMurdie, H. F., Eds.; American Ceramic Society: Westerville, OH, 1998.
(44) Morant, C.; Sanz, J. M.; Galán, L.; Soriano, L.; Rueda, F. *Surf. Sci.* **1989**, *218*, 331–345.
(45) Guittet, M. J.; Crocombette, J. P.; Gautier-Soyer, M. *Phys. Rev. B* **2000**, 63.
(46) Dzhurinskii, B. F.; Gati, D.; Sergushin, N. P.; Nefedov, V. I.; Salyn, Y. V. *Russ. J. Inorg. Chem.* **1975**, *20*, 2307–2314.
(47) Barr, T. L. *J. Phys. Chem.* **1978**, *82*, 1801–1810.
(48) Briggs, D.; Seah, M. P. *Practical Surface Analysis*, 2nd ed.; John Wiley & Sons: New York, 1993; Vol. 1.
(49) Ebert, H.; Knecht, M.; Muhler, M.; Helmer, O.; Bensch, W. *J. Phys. Chem.* **1995**, *99*, 3326–3330.

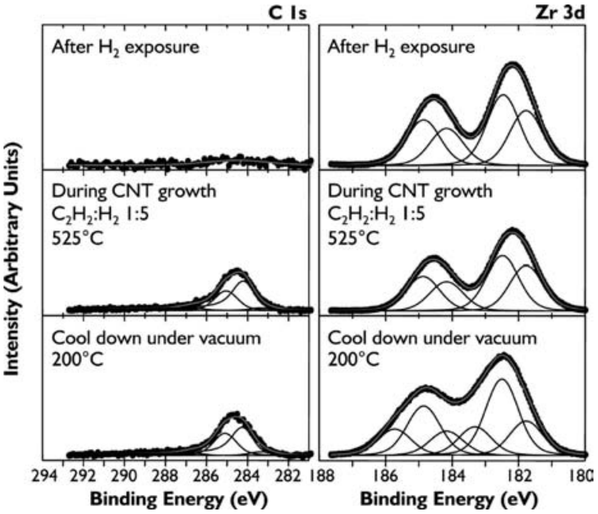

Figure 3. Progressive XPS snapshots of the C 1s and Zr 3d regions during growth of CNTs from zirconia on Si substrate. An appreciable carbon signal only appears upon introduction of both acetylene and hydrogen. No metallic zirconium or zirconium carbide is observed during growth.

and one with the Zr $3d_{5/2}$ peak at 181.8 eV. The lower binding energy signal is attributed to an oxygen-deficient phase of zirconia, while the higher binding energy signal is attributed to stoichiometric ZrO_2.[44] Thus, it appears that introduction of H_2 does not reduce the deposited zirconia film to Zr metal but instead pulls off residual chloride and alkoxide groups to yield oxide phases. Subsequent introduction of acetylene invokes an additional temporary, low-lying, high-binding energy signal attributed to a charging effect (also not shown). This signal disappears, and only signals corresponding to two phases of zirconia persist throughout the CVD growth. Upon addition of hydrogen to the acetylene stream, a C 1s peak emerges, which we attribute to nucleation of CNTs and possibly formation of other carbonaceous structures. This peak resolves into several components observed in CNT growth from other catalysts along with a low binding energy component located at 283.4 eV. This peak does not match the expected position for the C 1s peak of zirconium carbide (282 eV),[50,51] and so we speculate it may be caused by the interaction of a deposited organic with the support. Finally upon cool-down, only the two phases of zirconia observed during growth remain, along with a high binding energy signal attributed to charging effects. At no point prior, during, or after CVD growth of CNTs is metallic zirconium (binding energy 178.6−179.6 eV)[48,49,52] or zirconium carbide (binding energy 179−181.1 eV)[50,51] observed in the Zr 3d region. Thus, this confirms that the CNT growth catalyst is the oxide zirconia. Null CNT growth on zirconia-free Si substrates coated with alumina verified that the 10-nm alumina support layer is not serving as the catalyst, consistent with the findings of Mattevi et al. that continuous alumina films do not result in the growth of CNTs.[53]

Notably, the C 1s peak in the *in situ* XPS spectrum of the Si substrate did not appear immediately following introduction of acetylene but only after hydrogen was added as well. We speculate that the introduction of hydrogen aids in transformation of acetylene into other organic precursors that can then be uptaken and catalyzed into CNTs and/or other solid forms of carbon by zirconia. Perhaps common metallic CNT catalysts, such as Fe and Ni, are able to catalyze this hydrocarbon digestive process directly, which may explain why zirconia gives lower areal yields of CNTs.

We note that time-resolved, *in situ* XPS provides the most accurate information about the chemical state of the catalyst during CNT growth at that moment. Nevertheless, the question arises as to whether the active species during growth might be missed by XPS due to detection limits of species present in small quantities or because of short, transient changes in the state of a species on a time scale faster than the acquisition time. However, we argue that if such short and/or small atomic fraction processes do arise and result in traces of metallic or carbidic Zr, these traces would have been detectable at some point in the analysis as reduced Zr would not reoxidize in a vacuum and should not only remain detectable but also accumulate and become more detectable with time.

Raman spectroscopy was performed on the Si substrates used for the *in situ* XPS growth to assess the type and quality of CNTs that resulted from the growth.[54] Radial breathing modes between 130 to 280 cm^{-1} are observed within the XPS analysis area, indicating the presence of SWNTs (Figure 4). For an individual nanotube on an Si/SiO_2 substrate, the diameter of the nanotube in resonance with the laser can be approximated by d_t [nm] = 233 cm^{-1}/ω_{RBM}.[55] For the spectrum shown in Figure 4, nanotubes of 1.67, 1.18, and 0.84 nm are observed. The low D-to-G ratio suggests the presence of high-quality, low-defect CNTs. Raman peaks from zirconia[56] were not readily observable relative to carbon Raman peaks where CNTs were best resolved.

CNTs grown from zirconia nanoparticles during *in situ* XPS analysis were transferred onto TEM grids (Cu with C film) to verify that the XPS measurements are in fact representative of particles at the nanoscale and that zirconia nanoparticles are the catalyst responsible for CNT growth. CNTs attached to zirconia nanoparticles are observed (Figure 5). To further prove that the observed particles are in fact zirconia and not zirconium metal, we performed scanning transmission electron microscopy (STEM) and used point-localized energy-dispersive X-ray spectroscopy (EDAX) to characterize their elemental composition. EDAX reveals a stoichiometry of ~30% Zr and ~70% O for these nanoparticles, verifying a stoichiometry of ZrO_2 and further validating that our *in situ* and *ex situ* XPS and XRD characterizations are representative of the nanoscale. Multiple particles attached to multiple CNTs exhibit similar stoichiom-

---

(50) Won, Y. S.; Kim, Y. S.; Varanasi, V. G.; Kryliouk, O.; Anderson, T. J.; Sirimanne, C. T.; McElwee-White, L. *J. Cryst. Growth* **2007**, *304*, 324–332.

(51) Balaceanu, M.; Braic, M.; Braic, V.; Vladescu, A.; Negrilaa, C. C. *J. Optoelectron. Adv. Mater.* **2005**, *7*, 2557–2560.

(52) Moulder, J. F.; Stickle, W. F.; Sobol, P. E.; Bomben, K. D. *Handbook of X-Ray Photoelectron Spectroscopy*; Chastain, J., King, R. C., Jr., Eds.; Physical Electronics Division, Perkin-Elmer Corp.: Eden Prairie, MN, 1995.

(53) Mattevi, C.; Hofmann, S.; Cantoro, M.; Ferrari, A. C.; Robertson, J.; Castellarin-Cudia, C.; Dolafi, S.; Goldoni, A.; Cepek, C. *Phys. E (Amsterdam, Neth.)* **2008**, *40*, 2238–2242.

(54) Saito, R.; Grüneis, A.; Samsonidze, G. G.; Brar, V. W.; Dresselhaus, G.; Dresselhaus, M. S.; Jorio, A.; Cançado, L. G.; Fantini, C.; Pimenta, M. A.; Filho, A. G. S. *New J. Phys.* **2003**, *5*, 157.1157.15.

(55) Kurti, J.; Zolyomi, V.; Kertesz, M.; Sun, G. *New J. Phys* **2003**, *5*, 125.1125.21.

(56) Zyuzin, D. A.; Cherepanova, S. V.; Moroz, E. M.; Burgina, E. B.; Sadykov, V. A.; Kostrovskii, V. G.; Matyshak, V. A. *J. Solid State Chem.* **2006**, *179*, 2965–2971.

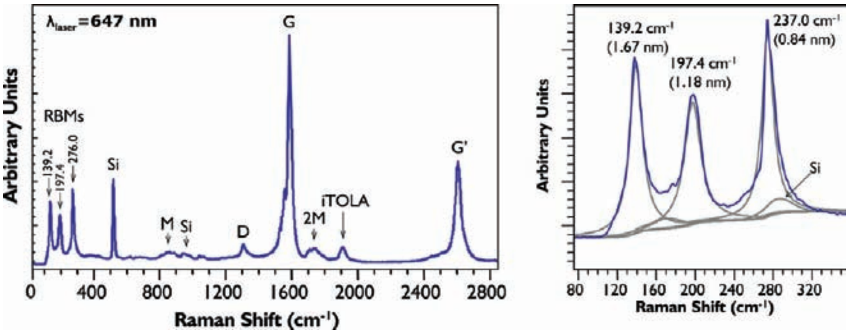

Figure 4. Raman spectrum from carbon nanotubes grown by CVD during *in situ* XPS analysis. The presence of radial breathing modes indicates the presence of single-wall carbon nanotubes.

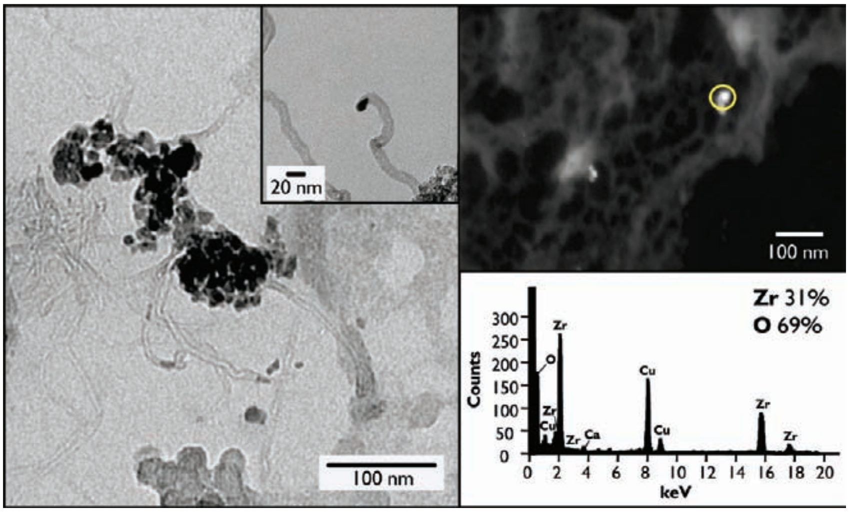

Figure 5. (*Left panel, main image*) TEM image of CNTs attached to zirconia catalyst nanoparticles from *in situ* XPS growth experiments (Cu with C film TEM grid); (*left panel, inset*) CNT attached to zirconia catalyst nanoparticle grown from zirconia-doped carbon aerogel; (*right, top*) scanning TEM (STEM) image of CNTs extending from zirconia nanoparticles grown during *in situ* XPS experiments; (*right, bottom*) representative point-localized EDAX spectrum of a nanoparticle (circled) attached to CNTs from *in situ* XPS experiment, verifying a particle composition of $\sim ZrO_2$.

etry. The ratio of oxygen to zirconium measured was consistent from particle to particle within ±5% and was not contributed by the grid or other structures on the grid as evidenced by EDAX spectra collected away from the particles of interest.

To better understand the interactions of nanoparticulate zirconia in the presence of carbon at elevated temperatures, zirconia nanoparticle-doped carbon aerogels were studied. A nanoparticle-doped carbon aerogel system offers several benefits for studying the interactions of nanoparticles of a material with carbon. First, it allows for synthesis of a bulk quantity of nanoparticles dispersed inside an amorphous carbon matrix for a wide range of nanoparticle compositions. Second, because the aerogel materials are macroscopic, three-dimensional monoliths, both bulk characterization techniques like XRD, which can be challenging to use for surface-bound particles, and surface analysis techniques like XPS can be used to characterize the nanoparticles of interest. Furthermore, the materials can be pyrolyzed over a wide range of temperatures, allowing for investigation of temperature dependency on the nanoparticle−carbon interactions.

Aerogels were prepared using an adapted version of the ion-exchange technique used to prepare metal-doped carbon aerogels. Metal-doped carbon aerogels prepared through ion exchange[37−39] typically exhibit a "blueberry muffin" morphology in which metal-containing nanoparticles ("blueberries") are dispersed throughout a low-density mesoporous amorphous carbon framework ("muffin"). In the case of Fe-[39] and Cu-doped[37] carbon aerogels, this carbon framework is essentially the same as in undoped carbon aerogels[57] for pyrolysis temperatures up to 1050 °C. During pyrolysis, the resorcinol−formaldehyde-type polymer framework of the aerogel dehydrates to afford amorphous carbon. Simultaneously, metal ions attached to the polymer framework are reduced and coarsen into a spectrum of metal-containing nanoparticles with a range of diameters and, depending on the metal, a range of crystallite phase and surface compositions. In similarly prepared Ni- and Co-doped carbon aerogels,[38] however, graphitic nanoribbons surrounding metal nanoparticles can be observed among an otherwise amorphous carbon matrix. In these materials the Ni and Co nanoparticles, which are both solvents for carbon, catalyze a solid-state transformation of the amorphous carbon into graphitic nanoribbons and other graphitic nanostructures.

The same ion-exchange process used to prepare metal-doped carbon aerogels was used to prepare ZrO_2-doped carbon aerogels, only employing $ZrOCl_2$ as the ion exchange salt. Carbon aerogels with an amorphous carbon structure laced with metallic Zr and/or ZrC nanoparticles were initially expected on the basis of results from the Fe-doped carbon aerogel system.

---

(57) Pekala, R. W.; Alviso, C. T.; LeMay, J. D. *J. Non-Cryst. Solids* **1990**, *125*, 67–75.

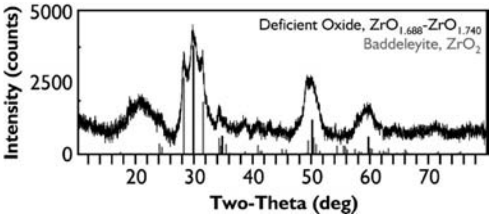

Figure 6. Powder XRD pattern of ZrO_2-doped carbon aerogels with possible phase matching corresponding to baddeleyite ZrO_2 (gray lines) and an oxygen-deficient phase of zirconia (black lines). The broad peak widths indicate the presence of nanosized crystallites (~7 nm average diameter). No peaks associated with Zr or ZrC are observed. The broad peak centered about 21° 2-θ is associated with the carbon component of the aerogel and is typical of carbon aerogels.

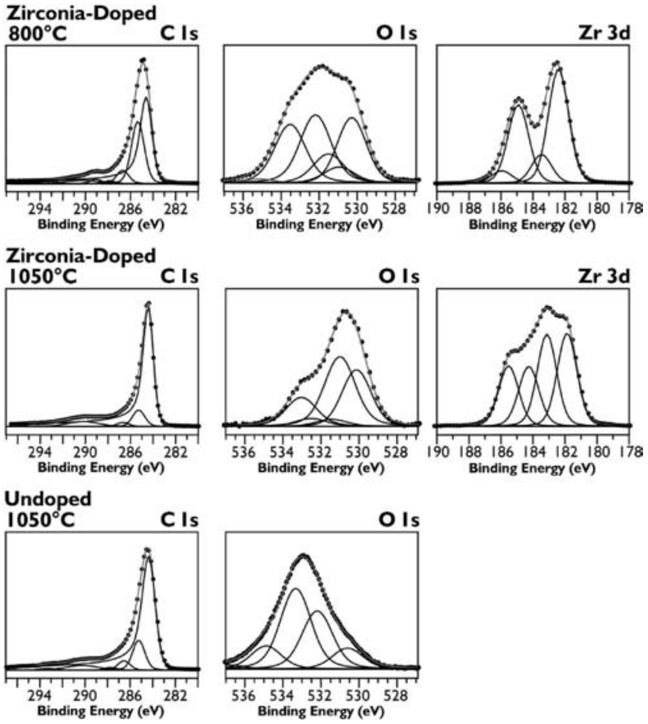

Figure 7. Representative XPS spectra of ZrO_2-doped carbon aerogels pyrolyzed at 800 °C (*top row*) and 1050 °C (*middle row*) and of undoped carbon aerogels pyrolyzed at 1050 °C (*bottom row*). Two chemistries of Zr are detected in both samples pyrolyzed at 800 °C and at 1050 °C, both exhibiting binding energies expected for zirconia. No signals attributable to Zr or ZrC (Zr $3d_{5/2}$ binding energies of 178−180 eV) could be found. Vertical axis is signal intensity in arbitrary units.

However, consistent with our observations of the irreducibility of zirconyl beyond oxygen-deficient zirconia during CNT growth, carbon aerogels laced with zirconia (ZrO_2) nanoparticles resulted instead. XRD of the ZrO_2-doped carbon aerogels (Figure 6) shows the presence of crystallites of zirconia in these materials. The diffraction pattern was phase matched to an oxygen-deficient phase of zirconia (with stoichiometry ranging from $ZrO_{1.688}$−$ZrO_{1.740}$)[58] superimposed over monoclinic baddeleyite zirconia (with stoichiometry ZrO_2).[59] The broad peak widths observed indicate the mean zirconia crystallite size is in the nanometer range and, using the Scherrer equation $d = 0.9\lambda/B \cos(\theta)$ to relate peak full-width at half-maximum values to crystallite size, an average crystallite size of ~7 nm is calculated.

Ex situ XPS analysis of the exterior and interior surfaces of ZrO_2-doped carbon aerogel monoliths (Figure 7) shows two pairs of spin−orbit-split peaks in the Zr 3d region for samples pyrolyzed at both 800 and 1050 °C, indicating the presence of two zirconia surface chemistries. In the sample pyrolyzed at 800 °C, the Zr $3d_{5/2}$ peak at 183.4 eV correlates to the binding energy for ZrO_2,[46−49] whereas the Zr $3d_{5/2}$ peak with a binding energy of 182.3 eV falls at a slightly lower binding energy than stoichiometric ZrO_2 and is likely an oxygen-deficient chemistry, ZrO_{2-x}. The lower binding energy chemistry is the dominant surface chemistry at 800 °C but gives way to a higher binding energy chemistry attributed to stoichiometric ZrO_2 at 1050 °C, possibly due to annealing. The lower binding energy chemistry also shifts down to 181.9 eV at 1050 °C, suggesting further oxygen deficiency. This is possibly due to migration of oxygen to form stoichiometric ZrO_2. Zr metal (binding energy 178.6−179.6 eV)[48,49,52] and ZrC (binding energy 178−179 eV)[51] were not observed after 100 sweeps. The O 1s region shows the presence of several chemistries of oxygen, including two at 530 eV and at 531 eV, which are consistent with the binding energies of oxygen in ZrO_2,[47] and one at 532.8−532.9 eV, which is also seen in undoped carbon aerogels and is attributed to oxygenated surface carbon on the aerogel framework. The presence of two non-carbon-aerogel oxygen chemistries and two zirconia chemistries supports the XRD pattern phase matches indicating the presence of two phases of zirconia, although there is likely a blend of substoichiometric surface oxides present in these samples. Furthermore, the low binding energy zirconia chemistries observed are consistent with the observation of an oxygen-deficient phase by XRD. The C 1s region for both ZrO_2-doped carbon aerogels and undoped carbon aerogels is essentially identical, and no peak attributable to ZrC in either the C 1s region (C 1s 282 eV) or Zr 3d region (179−181.1 eV) is observed.[50,51]

Observations regarding the surface and crystallographic composition of zirconia drawn from XRD and *ex situ* XPS of ZrO_2-doped carbon aerogels indicate that nanoparticulate ZrO_2 is not carbothermically reduced at temperatures up to 1050 °C, corroborating our observations from *in situ* XPS during CVD growth of CNTs. Furthermore, it is unlikely that these oxide nanoparticles result from, for example, Zr or ZrC formed during pyrolysis that are oxidized upon exposure to air. Other metal-doped carbon aerogels we have prepared (Cu,[60] Fe,[39] Ta,[15] Re,[15] and W[15] for example) all exhibit both metallic crystallites in their XRD patterns and detectable metallic surface chemistries in their XPS spectra long after exposure to air (months) in addition to oxide surface chemistries resulting from air exposure. Zr is less susceptible to oxidation than some of these metals, especially Fe; therefore, if reduced Zr was formed during pyrolysis, it would be detectable by either or both XRD and *ex situ* XPS after exposure to air.[61,62]

Investigation of ZrO_2-doped carbon aerogels under TEM (Figure 8) revealed the presence of fullerenic cage structures

---

(58) Matched to Inorganic Crystal Structure Database (ICSD) reference pattern file PDF00-049-1642 (ICDD Powder Diffraction File 4+); see: Tomaszewski, H.; Godwod, K. *J. Eur. Ceram. Soc.* **1995**, *15*, 17.

(59) Matched to Inorganic Crystal Structure Database (ICSD) reference pattern file PDF00-037-1484 (ICDD Powder Diffraction File 4+); see: McMurdie, H. F.; Morris, M.; Evans, E.; Paretzkin, B.; Wong-Ng, W.; Hubbard, C. R. *Powder Diffr.* **1986**, *1*, 265–275.

(60) Fu, R.; Yoshizawa, N.; Dresselhaus, M. S.; Dresselhaus, G.; Satcher, J. H., Jr.; Baumann, T. F. *Langmuir* **2002**, *18*, 10100–10104.

(61) Maitre, A.; Lefort, P. *Actual. Chim.* **1999**, *5*, 35–41.

(62) Gaskell, D. R. In *Encyclopedia of Materials: Science and Technology*; Buschow, K. H. J., Ed.; Elsevier: Amsterdam, New York, 2001; pp 5481−5486.

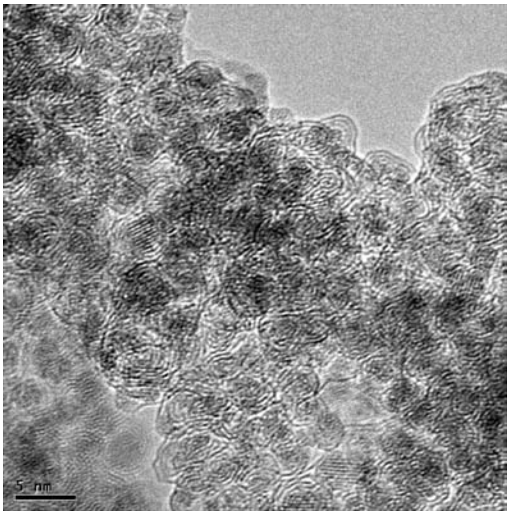

Figure 8. Fullerenic cage structures encasing zirconia nanoparticles in ZrO_2-doped carbon aerogel pyrolyzed at 800 °C. Such structures are not observed in undoped carbon aerogels.

encapsulating ZrO_2 nanoparticles. These types of structures are not observed in undoped carbon aerogels. Although graphitic nanoribbons have been reported in carbon aerogels doped with Ni and Co, these metals are solvents for carbon and are also known to act as low-temperature graphitizing catalysts. ZrO_2, however, has not been reported to act as graphitizing catalyst at 800 °C. Raman spectroscopy of ZrO_2-doped carbon aerogels at an excitation wavelength of 514 nm shows a broad D-band and broad G-band similar to those of undoped carbon aerogels. This suggests that the fullerenic structures in the aerogel are not representative of the entire aerogel framework but rather are localized around ZrO_2 nanoparticles in the aerogel, which only comprise ~2.9 at % of the aerogel structure as determined by *ex situ* XPS. These observations support the conclusion that zirconia can graphitize amorphous carbon.

ZrO_2-doped carbon aerogels were then assessed for activity toward catalyzing CNT growth via thermal CVD using ethylene feedstock at 700−750 °C. Tangled bundles of CNTs were observed covering the exterior surfaces of the ZrO_2-doped carbon aerogel monolith (Figure 9). TEM of CVD-processed ZrO_2-doped carbon aerogels verified the observed structures are in fact MWNTs (Figure 9, bottom). The MWNTs are found extending from zirconia nanoparticles in the carbon aerogel skeleton under TEM. No CNTs were observed on undoped carbon aerogels after processing with the same CVD growth conditions. These observations again suggest that the zirconia particles are serving as the CNT growth catalyst. XPS analysis of ZrO_2-doped carbon aerogels post-CVD revealed no detectable change in zirconium surface chemistry due to CNT growth, again consistent with the expectation that zirconia would not be reduced by hydrogen or carbon at the CNT growth temperatures. *In situ* XPS analysis of zirconia-doped carbon aerogels during CVD growth conditions further verified the absence of any metallic zirconium or zirconium carbide. Thus we conclude that the zirconia nanoparticles in the carbon aerogel are not reduced by the CVD growth process or from carbothermic reduction by the surrounding amorphous carbon, and serve as CNT catalysts in an oxide state. CNT yield on ZrO_2-doped carbon aerogels pyrolyzed at 1050 °C was noticeably lower than aerogels pyrolyzed at 800 °C. This finding suggests that the oxygen-deficient zirconia which is more prevalent in aerogels pyrolyzed at 800 °C is preferable for enabling CNT growth.

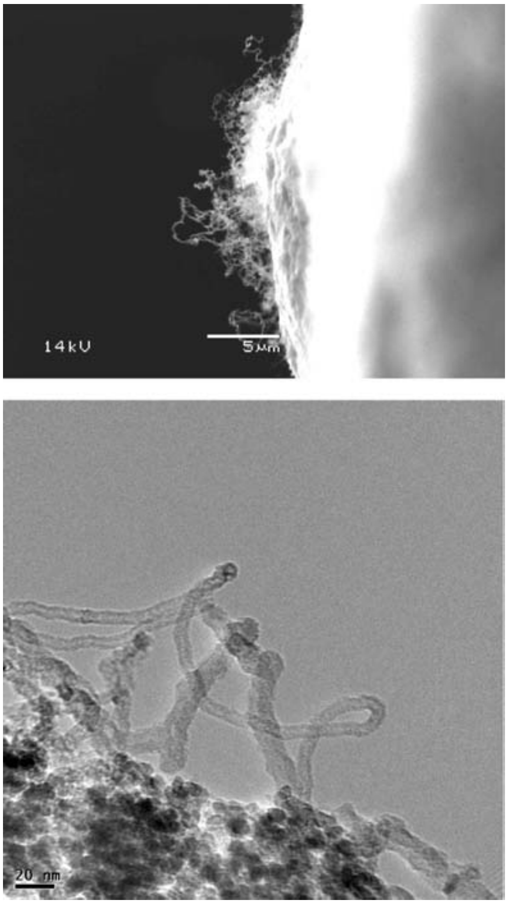

Figure 9. (*Top*) SEM image of multiwall carbon nanotubes protruding from the surface of a ZrO_2-doped carbon aerogel following CVD. (*Bottom*) TEM images of MWNTs emerging from zirconia nanoparticles embedded in ZrO_2-doped carbon aerogel (mass of circular particles in lower left region); scale bar is 20 nm.

Following the growth of CNTs from ZrO_2-doped carbon aerogels, CVD growth using zirconia on another carbon substrate, carbon fibers, was undertaken (see Supporting Information). Fiber tows were dip-coated with saturated $ZrOCl_2$ in 2-propanol solution, heated under H_2 to the growth temperature, and processed using CVD with ethylene as the feedstock gas as was done for the ZrO_2-doped carbon aerogels. Growth of CNTs is observed on the fibers following CVD; however, the growth is with nonuniform coverage. This proof-of-concept demonstrates the possibility of using ZrO_2 as a catalyst for substrates which react with metals at CNT growth temperatures such as carbon.

As we do in this study, a metal oxide support of a difficult-to-reduce oxide such as Al_2O_3, SiO_2, and occasionally MgO, TiO_2 or even ZrO_2 is often used in conjunction with a (typically metal) catalyst for CVD growth of CNTs. Common examples are Fe or Co/Mo on Al_2O_3.[63−66] While as highlighted earlier this is sometimes done to protect vulnerable substrates from unfavorable interaction with the catalyst, it is more commonly done to increase the percentage of suitably sized catalyst particles that result in CNT formation. In addition to providing

---

(63) Kong, J.; Soh, H. T.; Cassell, A. M.; Quate, C. F.; Dai, H. *Nature* **1998**, *395*, 878–881.

(64) Bachilo, S. M.; Balzano, L.; Herrera, J. E.; Pompeo, F.; Resasco, D. E.; Weisman, R. B. *J. Am. Chem. Soc.* **2003**, *125*, 11186–11187.

(65) Hart, A. J.; Slocum, A. H. *J. Phys. Chem. B* **2006**, *110*, 8250–8257.

(66) Maruyama, S.; Kojima, R.; Miyauchi, Y.; Chiashi, S.; Kohno, M. *Chem. Phys. Lett.* **2002**, *360*, 229–234.

a textured surface for limiting the rate of catalyst coarsening,[53] many believe the metal oxide somehow enhances (or "promotes") the actual activity of the catalyst. Interestingly, oxygen-deficient (nonstoichiometric) alumina (AlO_x as opposed to Al_2O_3), has been shown to be the preferred phase for enhancing catalytic activity in the case of CNT growth in water-assisted growth from alumina-supported Fe.[67] Mattevi et al., however, show that neither alumina nor oxygen-deficient alumina films dissociate acetylene directly, which indicates that any enhancement in catalytic activity resulting from such oxide supports must arise from interactions with the catalyst directly.[53] Also notably, the effectiveness of oxides as heterogeneous catalysts (for example in hydrocarbon reforming) is known to be closely related to the electronic and defect properties of the oxide.[68−70] Electron transfer between catalyst and reactant(s) depends heavily on the ability of the catalyst to accept or donate excess electrons or positive charges, which dangling bonds on defective oxides can help facilitate.[69,71] Zirconia is used as a catalyst in the decomposition of nitrous oxide[72] and in the synthesis of dimethyl carbonate from methanol and carbon dioxide[73] in which Zr^{3+} and Zr^{4+} cations in the zirconia particle lattice facilitate catalysis by serving as sites for molecular absorption and allowing for temporary bonding configurations with incoming substrate molecules. Interestingly, chemisorption of various intermediate gas-phase species (i.e., oxygen and carbene) is known to occur more readily on n-type oxides.[69] As we have observed the presence of oxygen-deficient zirconia by both XPS and XRD in catalysts used in this work, it is interesting to consider that defect properties may play a role in the catalytic activity of nanoparticulate zirconia. The H_2 pretreatment in this work, while shown not to result in metallic Zr, may play a role in introducing surface defect sites onto zirconia nanoparticles that aid in enhancing catalytic activity. Additionally, as observed through *in situ* XPS, CNT growth seems to begin only upon introduction of both hydrocarbon and hydrogen, which might be due to introduction of defects by transient, localized extraction of oxygen by hydrogen. Presence of high-surface energy features (such as nanoparticles) and deposition technique are also potential variables which may affect defects. Understanding the role of defect properties of zirconia as a graphitizing catalyst and CNT growth catalyst may provide insights into the function of difficult-to-reduce oxides in their roles as catalyst supports for CNT growth.

The high melting point of bulk ZrO_2 makes it unlikely that nanoscale ZrO_2 exists in a molten state at the CVD growth temperatures used here, even after factoring in particle size effects. Additionally, given the low diffusivity of C in bulk ZrO_2, the successful growth of CNTs and graphitic nanoshells by ZrO_2 demonstrated here is suggestive of CNT growth by a surface-borne mechanism. We hypothesize that, like Fe, zirconia may catalyze reactions of organic molecules on its surface that aid in the assembly of the nanotube/nanoshell structure; however, zirconia may involve intermediates and bonding configurations different than Fe and other metals. Further studies are underway to test this hypothesis.

Conclusions

We conclude that the oxide zirconia is a catalyst for thermal CVD growth of CNTs and can catalyze both SWNT and MWNT growth, in some cases with enough activity to create forest morphologies of CNTs. We also conclude that nanoparticulate zirconia can catalyze transformation of amorphous carbon into a graphitic form. As seen from *in situ* XPS analysis of CNT growth from zirconia, zirconia appears to be the active CNT catalyst species and does not reduce to metallic zirconium or zirconium carbide under the CVD growth conditions. These discoveries provide valuable perspective on the nature of CNT growth catalysts, as it appears conclusively, for the first time, that an oxide which is not reducible under CNT growth conditions can catalyze CNT growth. We hypothesize that oxygen-deficient zirconium oxide may be more active than stoichiometric zirconia. We note that ZrO_2, like Al_2O_3, SiO_2, and TiO_2, is also sometimes used as a catalyst support in heterogeneous catalysis of hydrocarbons and hypothesize that its function in these applications may be related to the catalytic activity we observe here. Furthermore, zirconia offers unique potential as a useful catalyst for substrates that are susceptible to damage by metallic CNT growth catalysts, for example, carbon substrates like carbon fibers used in composites.

It is interesting to consider fuel cells that employ yttria-stabilized zirconia (YSZ) as a solid electrolyte for understanding more about the behavior of zirconia as a catalyst. In these fuel cells, the triple-phase boundary of cathode metal, metal oxide, and hydrocarbon − not just the metal−hydrocarbon interface − serves as the catalytic center of activity for the extraction of electrons and concomitant transformation of hydrocarbons into carbon dioxide.[74] Such interfaces are also susceptible to poisoning by coking-over, which may be related to the catalytic propensity of nanoparticulate zirconia described in this study.

Finally, we have also made initial observations of CNT growth from hafnia (HfO_2), and are working to understand the catalytic propensity of this and other metal oxides as well.

Acknowledgment. We thank Dr. Desirée Plata for helpful discussions and review, Namiko Yamamoto and Dr. Woo-Sik Kim for conducting e-beam depositions, Dr. Roberto Guzmán de Villória, Megan Tsai, and Richard Li for assistance in parametric growth studies, Alfonso Reina and Federico Villalpando for assistance in obtaining Raman spectra, Dr. Scott Speakman for assistance in acquiring XRD patterns, Susie Evans for her time-critical assistance in obtaining XPS spectra, and the technical support staff at BESSY for their assistance in conducting *in situ* XPS CVD growth experiments. We also thank TohoTenax Corporation and Hexcel Coporation for their donation of carbon fiber and Aerogel Technologies, LLC, for use of their supercritical dryers. S.H. acknowledges funding by the Royal Society and Peterhouse, Cambridge. This work was supported by Airbus S.A.S., Boeing, Embraer, Lockheed Martin, Saab AB, Spirit AeroSystems, Textron Inc., Composite Systems Technology, and TohoTenax through MIT's Nano-Engineered Composite aerospace STructures (NECST) Consortium. This work made use of the Shared Experimental Facilities in the MIT Center for Materials Science and Engineering supported by the MRSEC Program of the National Science Foundation under

---

(67) Noda, S.; Hasegawa, K.; Sugime, H.; Kakehi, K.; Zhang, Z.; Maruyama, S.; Yamaguchi, Y. *Jpn. J. Appl. Phys., Part 2* **2007**, *46*, L399–L401.

(68) Wal, R. L. V.; Ticich, T. M.; Curtis, V. E. *Carbon* **2001**, *39*, 2277–2289.

(69) Hauffe, K. *DECHEMA Monogr.* **1956**, *26*, 301–32.

(70) Satterfield, C. N. *Heterogeneous Catalysis in Industrial Practice*, 2nd ed.; McGraw-Hill: New York, 1991.

(71) Freund, H.-J. *Surf. Sci.* **2007**, *601*, 1438–1442.

(72) Miller, T. M.; Grassian, V. H. *Catal. Lett.* **1997**, *46*, 213–221.

(73) Tomishige, K.; Sakaihori, T.; Ikeda, Y.; Fujimoto, K. *Catal. Lett.* **1999**, *58*, 225–229.

(74) Singhal, S. C.; Kendall, K., Eds. *High Temperature Solid Oxide Fuel Cells: Fundamentals, Design, and Applications*; Elsevier: Oxford, New York, 2003.

Award Number DMR 02-13282. This work was supported by the European Community Research Infrastructure Action under the FP6 "Structuring the European Research Area" Programme (through the "Integrated Infrastructure Initiative" Integrating Activity on Synchrotron and Free Electron Laser Science, Contract R II 3-CT-2004-506008).

Supporting Information Available: SEM images of CNTs grown from zirconia nanoparticle catalysts on carbon fibers. This material is available free of charge via the Internet at http://pubs.acs.org.

JA902913R